PERGAMON

International Journal of Solids and Structures 39 (2002) 3935–3957

INTERNATIONAL JOURNAL OF SOLIDS and STRUCTURES

www.elsevier.com/locate/ijsolstr

Thermopiezoelectric response of a piezoelectric thin film PZT-6B deposited on MgO(100) substrate due to a continuous laser

X.J. Zheng [a,b], Y.C. Zhou [a,*], M.Z. Nin [b]

[a] *Institute of Fundamental Mechanics and Material Engineering, Xiangtan University, Xiangtan, Hunan, 411105, China*
[b] *Department of Mathematics, Physics and Mechanics, Central South University, Changsha 410075, China*

Received 26 November 2001; received in revised form 26 March 2002

Abstract

Laser irradiation of piezoelectric thin film produces a heating effect due to the absorption of light energy. In this paper, a theoretical model is proposed to study thermopiezoelectric response of piezoelectric thin film. The transient heat transfer equation with two-dimensional composite media is analytically solved by employing integral transform technique. The thermopiezoelectric problem of piezoelectric thin film induced by laser beam is studied by means of potential function method. In this case, the fields of stress, displacement and electric displacement are analytically obtained and the general analytical solutions in quasi-static are written by a double series with dimensionless of formulation. The numerical results of thermopiezoelectric fields for a piezoelectric thin film PZT-6B deposited on MgO(100) substrate induced by Gaussian or doughnut laser beam are obtained and the results are discussed.

The calculated results show that temperature field is determined by the characteristic beam radius d and the maximum incident flux for Gaussian source q_0. The radial and circumferential stresses in the thin film PZT-6B are tensile and much larger than normal (compressive) and shear stresses. The Gaussian laser beam heating will produce higher radial and circumferential stresses, however, the doughnut source will produce higher normal and shear stresses. The horizontal electric displacement in the thin film is much larger than the vertical electric displacement.

Keywords: Piezoelectric thin film; Thermopiezoelectric fields; Laser pulse; Piezoelectric potential function

1. Introduction

Piezoelectric thin film materials has developed rapidly in recent years due to its wide application, including high-value capacitors, infrared detectors, sensors and actuators, optical switches, ferroelectric field-effect transistors, non-volatile memories (Haertling, 1999; Kant, 1988). Lead-zirconate–titanate $Pb(Zr_xTi_{1-x})O_3$ (PZT) thin films have been intensively investigated for such applications. The PZT

* Corresponding author. Tel.: +86-732-829-3586; fax: +86-732-829-2468.
E-mail addresses: yichunzhou@hotmail.com, zhouyc@xtu.edu.cn (Y.C. Zhou).

0020-7683/02/$ - see front matter
PII: S0020-7683(02)00268-8

ferroelectric memory has many advantages such as high density, retention of charge over long periods of time (order of decades) with any supplied voltage, and radiation immunity. Since these PZT materials have dielectric constants, their application as dielectric layers in extreme high density, new generation dynamic random access memory looks promising. The PZT thin films have been fabricated by various techniques such as pulsed laser ablation (Verardi et al., 1997), rf sputtering (Choi et al., 1999), chemical vapor deposition (Sakashita et al., 1991), metallo-organic decomposition (Zhu et al., 1996), sol–gel process(Cheng et al., 2000).

However, as we know, it is natural that the film may fail due to the heating load, electric load as well as mechanical load in the case of the film at operating state. Much research has shown that the compressive stress may cause the film delamination from substrate. The tensile stress in thin film may cause the surface crack in film (Hutchinson and Suo, 1992; Evans and Hutchinson, 1995). Piezoelectric thin film materials operating in many structural components, especially aerospace components are ineluctable subject to severe thermal loading which may be produced by aerodynamic heating, by laser irradiation, or by localized intense fire (Duan et al., 1995; Zhou et al., 1997). In order to study the failure characteristics of PZT thin film at heating load, the fields such as displacement, temperature and stress should be first known. The piezoelectric actuator model and composite beam model are proposed to study coating or thin film system (Wang and Meguid, 2000; Zhou and Hashida, in press). Because of their inherent complexity, relatively few solutions for such coupled problems are available in the literatures.

Pulsed laser is now commonly used in such diverse applications, as drilling, welding, hardening, quenching, cutting and thin film technology. Laser irradiation produces a heating effect due to the absorption of light energy (Nonhof, 1988; Steen, 1991; Welsh et al., 1988; Volchenok and Rudin, 1988). Theoretical and experimental investigations of laser heating of materials and the resulting thermal stress fields began to appear not long after the laser became a significant materials processing tool. Volchenok and Rudin (1988) derived thermal stress field in a multiple plate due to the action of a continuous Gaussian surface source. Hector and Hetnarski (1996) derived the thermal stress field in elastic half-space due to a single pulse from a laser for the general case of a mixed-mode structure beam. The effect of laser spatial distribution on the failure mechanism of materials is comprehensively investigated by Zhou and Duan (Duan et al., 1996; Zhou and Duan, 1996). A tendency to develop critical crack growth because of stress concentrations induced by mechanical and/or electric and/or thermal loads, have a dominant influence on the failure of components (Crawley and de Luis, 1987; Im and Atluri, 1989).

The objective of the present paper is to propose an analytical model of thermopiezoelectric response of a piezoelectric thin film and to obtain analytically stress fields due to pulsed laser heating for the piezoelectric thin film. This research is significant in the life prediction and failure mechanism study for piezoelectric thin film system operating at heating environment. Employing integral transfer technique and piezoelectric potential function method, temperature and thermopiezoelectric fields in piezoelectric thin film are derived respectively. If the parameters of laser beam, materials and geometry are known, a dimensionless numerical result of the fields in the piezoelectric thin film PZT-6B deposited on MgO(1 0 0) substrate is obtained by MATLAB standard routine. The effect of the stress field on the damage/failure is also discussed.

2. Theoretical model

2.1. Statement of the problem

For the study of failure mechanism of a piezoelectric thin film system operating at laser irradiation condition, the physical map of temperature, thermal stress and electric fields should be first understood. Generally, the problem should be three-dimensional. For simplicity, a system of cylindrical coordinates for two-dimensional case is studied. Let us now consider a thermopiezoelectric model that comprises two layers

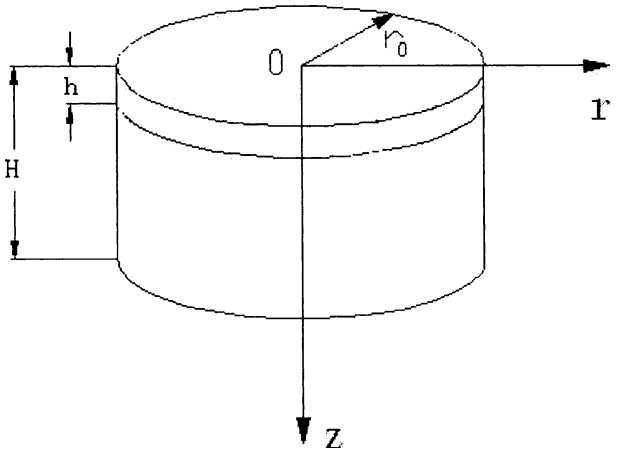

Fig. 1. Schematic of the theoretical model for the piezoelectric response in PZT thin film induced by laser beam.

in solid cylinder ($0 < r < r_0$), thin film with thickness h and substrate with thickness H, the cylindrical symmetry model consists of a piezoelectric thin film deposited on a crystal substrate as schemed in Fig. 1. The deformation in radial direction is much large than that in the perpendicularity direction due to the fact that the thickness of piezoelectric thin film is much small than the radius. Therefore, it is logical to have the following assumptions:

(i) Heat flux is absorbed in the outer surface and there is not heat source in the bodies.
(ii) The heat flux across interface is continuous and the interface is completely heat contact.
(iii) There is not body force, nor body charge.
(iv) Thermopiezoelectric fields are quasi-static, non-coupled.
(v) The substrate is rigidity along perpendicularity direction, i.e. along z-direction. The axial displacement at interface is zero.

2.2. Temperature fields

2.2.1. Governing equations

The heat conductivity equations for the transient temperature field $T_i(r,z,t)$ in thin film and substrate can be written as

$$\frac{\partial^2 T_i}{\partial r^2}+\frac{1}{r}\frac{\partial T_i}{\partial r}+\frac{\partial^2 T_i}{\partial z^2}=\frac{1}{\alpha_i}\frac{\partial T_i}{\partial t}, \quad 0<r<r_0, \ \ i=1,2, \tag{1}$$

where $i = 1, 2$ denotes thin film and substrate, respectively. The boundary conditions for temperature and heat flux can be expressed as in the following:

$$\left.\begin{aligned} &-k_1\frac{\partial T_1}{\partial z}\Big|_{z=0,r\leqslant r_0}=f_1(r,t), && \frac{\partial T_2}{\partial z}\Big|_{z=H,r\leqslant r_0}=0,\\ &\frac{\partial T_1}{\partial r}\Big|_{0<z<h,r=r_0}=0, && \frac{\partial T_2}{\partial r}\Big|_{0<z<h,r=r_0}=0,\\ &T_1|_{z=a,r\leqslant r_0}=T_2\Big|_{z=a,r\leqslant r_0}, && k_1\frac{\partial T_1}{\partial z}\Big|_{z=h,r\leqslant r_0}=k_2\frac{\partial T_2}{\partial z}\Big|_{z=h,r\leqslant r_0}. \end{aligned}\right\} \tag{2}$$

The initial conditions can be expressed as

$$T_i(r,z,t)|_{t=0} = T_0 = 0 \quad z_{i-1} \leqslant z < z_i, r \leqslant r_0 \tag{3}$$

In Eqs. (1)–(3), k_i, $\alpha_i = k_i/\rho_i c_{pi} (i = 1,2)$ is, respectively, thermal conductivity and thermal diffusivity, t is time, and ρ_i, c_{pi} $(i = 1,2)$ is the density and the specific heat coefficient, respectively. The term $f_1(r,t) = Y(t)Q(r)$ is heat flux on the outer surface, where $Y(t)$ and $Q(r)$ are, respectively, the temporal and spatial distributions. In the present paper, the temporal distribution of laser beam is chosen as $Y(t) = 1$. It means that the problem is stationary. The following function is chosen to represent the heat absorbed on the surface due to a pulsed laser with a mixed-mode structure (Hector and Hetnarski, 1996):

$$Q(r) = q_0 \left[f + (1-f)\left(\frac{r}{d}\right)^2 \right] \mathrm{e}^{-(r/d)^2}. \tag{4}$$

The parameters d and q_0 are the characteristic beam radius and the maximum incident flux for Gaussian source, respectively. Here, $f = 1$ and $f = 0$ denote that laser beam is Gaussian source and doughnut source, respectively. Fig. 2 schematics the spatial distributions of laser beam with Gaussian source and doughnut source.

2.2.2. Solution of temperature fields

The above equations about temperature field are a problem with non-homogeneous boundary conditions. Generally, the orthogonal expansion technique is used to solve the homogeneous problem of composite medium of finite thickness (Özisik, 1993). The solution of temperature fields in general form can be given as

$$T_i(r,z,t) = \sum_{m=1}^{\infty} \sum_{n=1}^{\infty} A_0(\beta_m, \lambda_n, t) R_0(\beta_m, r) Z_{i,n}(\beta_m, \lambda_n, z), \quad i = 1,2, \tag{5}$$

where the coefficient $A_0(\beta_m, \lambda_n, t)$, the fundamental functions $R_0(\beta_m, r)$, $Z_{i,n}(\beta_m, \lambda_n, z)$, normal number $N(\beta_m, \lambda_n)$ and characteristic values β_m, λ_n are given in Appendix A.

2.2.3. Dimensionless formulation of temperature fields

If the initial temperature T_0 is chosen as the reference temperature, temperature fields can be rewritten as

$$\Theta_i = T_i - T_0 \quad i = 1,2. \tag{6}$$

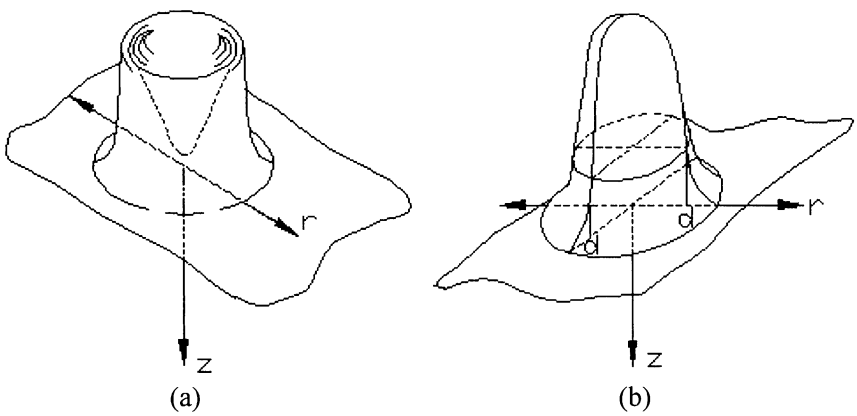

Fig. 2. Mode structure of laser source: (a) Doughnut source ($f = 0$), (b) Gaussian source ($f = 1$).

The physical variables are written in a non-dimensional form as in the following:

$$\begin{aligned} &r^* = \frac{r}{d}, \quad z^* = \frac{z}{d}, \quad r_0^* = \frac{r_0}{d}, \quad z_h^* = \frac{h}{d}, \quad z_H^* = \frac{H}{d}, \quad \beta_m^* = \beta_m d, \quad \lambda_n^* = \frac{\lambda_n d}{\sqrt{\alpha_1}}, \\ &t^* = \frac{\alpha_1 t}{d^2}, \quad \tau^* = \frac{\alpha_1 \tau}{d^2}, \quad \Theta_1^* = \frac{r_0^2 k_1}{2q_0 d^3} T_1, \quad \Theta_2^* = \frac{r_0^2 k_1}{2q_0 d^3} T_2, \quad A_0^* = \frac{r_0^2 k_1}{2q_0 d^3} A_0. \end{aligned} \tag{7}$$

The solution of temperature fields (5) may be rewritten in dimensionless form as

$$\Theta_1^* = \sum_{m=1}^{\infty} \sum_{n=1}^{\infty} A_0^*\left(\beta_m^*, \lambda_n^*, t^*\right) J_0\left(\beta_m^* r^*\right) \cos \sqrt{\left(\lambda_n^{*2} - \beta_m^{*2}\right)} z^*, \tag{8}$$

$$\begin{aligned} \Theta_2^* = \sum_{m=1}^{\infty} \sum_{n=1}^{\infty} A_0^*\left(\beta_m^*, \lambda_n^*, t^*\right) J_0\left(\beta_m^* r^*\right) \Bigg\{ & \cos \sqrt{\left(\lambda_n^{*2} - \beta_m^{*2}\right)} z_h^* \cos \sqrt{\left(\alpha \lambda_n^{*2} - \beta_m^{*2}\right)} \left(z_h^* - z^*\right) \\ & + K \frac{\sqrt{\left(\lambda_n^{*2} - \beta_m^{*2}\right)}}{\sqrt{\left(\alpha \lambda_n^{*2} - \beta_m^{*2}\right)}} \sin \sqrt{\left(\lambda_n^{*2} - \beta_m^{*2}\right)} z_h^* \sin \sqrt{\left(\alpha \lambda_n^{*2} - \beta_m^{*2}\right)} \left(z_h^* - z^*\right) \Bigg\}, \end{aligned} \tag{9}$$

where, $\alpha = \frac{\alpha_1}{\alpha_2}$, $\gamma = \frac{\rho_2 c_{p2}}{\rho_1 c_{p1}}$, $K = \frac{k_1}{k_2}$.

2.3. Thermopiezoelectric fields

2.3.1. Governing equations

As mentioned in the above, the substrate is rigid and therefore, the film is focused in the section. The governing equations of thermopiezoelectric medium were first derived and commonly used in studying piezoelectric materials (Mindlin, 1974; Nowacki, 1978; Iesan, 1989). The three-dimensional theory of thermopiezoelectricity in the absence of body forces and free charges can be written in a compact manner as following (Mindlin, 1974):

$$\left.\begin{aligned} \sigma_{ij} &= C_{ijkl}\varepsilon_{kl} - e_{kij}E_k - \lambda_{ij}\Theta, \\ D_i &= e_{ikl}\varepsilon_{kl} + \epsilon_{ik}E_k + p_i\Theta, \\ S &= \lambda_{kl}\varepsilon_{kl} + p_k E_k + \eta\Theta, \end{aligned}\right\} \quad \left.\begin{aligned} &\sigma_{ij,j} = 0, \\ &D_{i,i} = 0, \\ &h_{i,i} = -T_0 S, \end{aligned}\right\} \quad \left.\begin{aligned} \varepsilon_{ij} &= \tfrac{1}{2}(u_{i,j} + u_{j,i}), \\ E_i &= -\varphi_{,i}, \\ h_i &= -k_{ij}T_{,j}, \end{aligned}\right\} \tag{10}$$

where $i, j, k, l = 1, 2, 3$ and σ_{ij}, D_i, ε_{ij}, u_i, E_i, φ, h_i and S are the components of stress, electric displacement, strain, displacement, electric field, electric potential, heat flux and entropy density, respectively. The term $\Theta = T - T_0$ is a temperature change with reference temperature T_0. In Eq. (10), η is thermal expansion coefficient. The coefficients C_{ijkl}, ε_{ik}, e_{kij}, λ_{ij} and p_i are elastic, dielectric, piezoelectric, thermal modulus and pyroelectric coefficients, respectively.

For a transversely isotropic thermoelectromechanical body, the constitutive relations become tractable if we introduce a system of cylindrical coordinates (r, θ, z) for three-dimensional axisymmetric case. Noting that the corresponding components are functions of r and z, independent of the angle of θ and $u_\theta = 0$, the equilibrium equations are given in the form of elastic displacement, electric potential and temperature change. The details are given in Appendix B.

2.3.2. Determination of piezoelectric potential functions

Referring the previous research (Ashida et al., 1994; Wang and Zheng, 1995; Shang et al., 1996; Zhao et al., 1997), we introduce the following representation in terms of four potential functions ψ, ψ_1, ψ_2 and ψ_3:

$$\left.\begin{aligned} u &= \tfrac{\partial}{\partial r}(\psi_1+\psi_2+\psi_3+\psi),\\ w &= \tfrac{\partial}{\partial z}(l_{11}\psi_1+l_{12}\psi_2+l_{13}\psi_3+l_{14}\psi),\\ \varphi &= \tfrac{\partial}{\partial z}(l_{21}\psi_1+l_{22}\psi_2+l_{23}\psi_3+l_{24}\psi), \end{aligned}\right\} \tag{11}$$

where l_{ij}, $i = 1, 2$, $j = 1, 2, 3, 4$ are some constant coefficients which is determined in Appendix B.

Due to the special form of temperature field $T_1(r,z,t)$ in thin film as obtained in the above, the potential function $\psi(r,z)$ can be written in the following form:

$$\psi(r,z) = \sum_{m=1}^{\infty}\sum_{n=1}^{\infty} A_0(\beta_m,\lambda_n,t) D_m(\beta_m,\lambda_n) J_0(\beta_m r)\cos\sqrt{\left(\frac{\lambda_n^2}{\alpha_1}-\beta_m^2\right)}z, \tag{12}$$

where $D_m(\beta_m,\lambda_n)$ is a function of (β_m,λ_n) which are related with l_{14}, l_{24}. The potential function $\psi(r,z,t)$ is determined by the following equation,

$$\frac{\partial^2\psi}{\partial r^2}+\frac{1}{r}\frac{\partial\psi}{\partial r}+\frac{\partial^2\psi}{\partial z^2}=\frac{\partial\psi}{\partial t} \quad \psi=\psi_4. \tag{13}$$

Considering the quasi-static assumption in the theoretical model, one has the equation $\partial\psi/\partial t = 0$ and the assumption is as same as the discussion of Hector and Hetnarski (1996). The potential functions $\psi_j (j = 1,2,3)$ satisfy the homogeneous equations

$$\frac{\partial^2\psi_j}{\partial r^2}+\frac{1}{r}\frac{\partial\psi_j}{\partial r}+\gamma_j^2\frac{\partial^2\psi_j}{\partial z^2}=0. \tag{14}$$

It is natural that the force in the free surface is zero, i.e. $\sigma_{zr}\equiv 0$ at $z = 0$, therefore, ψ_j can be expressed as follows:

$$\left.\begin{aligned} \psi_1(r,z_1) = {} & \tfrac{\gamma_1}{a_1}\sum_{m=1}^{\infty} J_0(\beta_m r)[A_1 sh(\beta_m z_1)+B_1 ch(\beta_m z_1)]\\ \psi_2(r,z_2) = {} & \tfrac{\gamma_2}{a_2}\sum_{m=1}^{\infty} J_0(\beta_m r)[A_2 sh(\beta_m z_2)+B_2 ch(\beta_m z_2)]\\ \psi_3(r,z_3) = {} & -\tfrac{\gamma_3}{a_3}\sum_{m=1}^{\infty} J_0(\beta_m r)[A_1 sh(\beta_m z_3)+B_1 ch(\beta_m z_3)]\\ & -\tfrac{\gamma_3}{a_3}\sum_{m=1}^{\infty} J_0(\beta_m r)[A_2 sh(\beta_m z_3)+B_2 ch(\beta_m z_3)]\\ & -\tfrac{\gamma_3}{a_3}\tfrac{a_4}{\kappa}\sum_{m=1}^{\infty}\sum_{n=1}^{\infty} A_0(\beta_m,\lambda_n,t) D_m J_0(\beta_m r)\cos\sqrt{\left(\tfrac{\lambda_n^2}{\alpha_1}-\beta_m^2\right)}z_3 \end{aligned}\right\} \tag{15}$$

$$z_i=\frac{z}{\gamma_i} \quad (i=1,2,3) \qquad z_4=\frac{z}{\kappa} \quad \kappa=1,$$

where the functions $A_1(\beta_m)$, $B_1(\beta_m)$, $A_2(\beta_m)$, $B_2(\beta_m)$ will be determined by the force boundary conditions and the discussions will be given in the following. The corresponding factors γ_j, a_i are defined in Appendix B.

2.3.3. Potential function expression of thermopiezoelectric fields

The solution of governing Eq. (10) can be represented by three quasi-harmonic functions $\psi_j (j = 1, 2, 3)$ and one non-homogeneous function ψ. Substituting the representation in terms of four potential functions (11) into the constitutive Eq. (10), the corresponding stress and electric displacement components are obtained and they are given as follows

$$\left.\begin{aligned}
\sigma_{rr} &= \sum_{j=1}^{4}\left[c_{11}\psi_{j,rr} + c_{12}\tfrac{1}{r}\psi_{j,r} + \left(c_{13}l_{1j} + e_{31}l_{2j}\right)\psi_{j,zz}\right] - \lambda_{11}\Theta_1,\\
\sigma_{zz} &= \sum_{j=1}^{4}\left[c_{13}\left(\psi_{j,rr} + \tfrac{1}{r}\psi_{j,r}\right) + \left(c_{33}l_{1j} + e_{33}l_{2j}\right)\psi_{j,zz}\right] - \lambda_{33}\Theta_1,\\
\sigma_{zr} &= \sum_{j=1}^{4}\left(c_{44} + c_{44}l_{1j} + e_{15}l_{2j}\right)\psi_{j,rz},\\
\sigma_{\theta\theta} &= \sum_{j=1}^{4}\left[c_{12}\psi_{j,rr} + c_{11}\tfrac{1}{r}\psi_{j,r} + \left(c_{13}l_{1j} + e_{31}l_{2j}\right)\psi_{j,zz}\right] - \lambda_{11}\Theta_1,\\
D_r &= \sum_{j=1}^{4}\left[e_{15}\left(1 + l_{1j}\right) - \epsilon_{11}l_{2j}\right]\psi_{j,rz} + p_1\Theta_1,\\
D_z &= \sum_{j=1}^{4}\left[e_{31}\left(\psi_{j,rr} + \tfrac{1}{r}\psi_{j,r}\right) + \left(e_{33}l_{1j} - \epsilon_{33}l_{2j}\right)\psi_{j,zz}\right] + p_3\Theta_1.
\end{aligned}\right\} \tag{16}$$

2.3.4. Dimensionless formulation of thermopiezoelectric fields

In order to obtain the dimensionless solutions for the fields of stress, displacements and electric displacements, we define the following variables,

$$G = \frac{2q_0\lambda_{33}d^3}{r_0^2k_1}, \quad F = \frac{2q_0p_3d^3}{r_0^2k_1}, \quad DD = \frac{\lambda_{11}a_4}{\lambda_{33}(c_{11} - M_4)}. \tag{17}$$

When the dimensionless variables defined in expressions (7) are used and the Eqs. (12) and (15) are substituted into the former four formulas of Eq. (16), the dimensionless formulation of stress fields are obtained as

$$\begin{aligned}
\sigma_{zz}^* = \frac{\sigma_{zz}}{G} &= \sum_{m=1}^{\infty}\beta_m^{*2}J_0\left(\beta_m^*r^*\right)\left\{\frac{b_1}{a_1\gamma_1}\left[A_1^*sh\left(\beta_m^*z_1^*\right) + B_1^*ch\left(\beta_m^*z_1^*\right)\right] - \frac{b_3}{a_3\gamma_3}\left[A_1^*sh\left(\beta_m^*z_3^*\right) + B_1^*ch\left(\beta_m^*z_3^*\right)\right]\right.\\
&\left. + \frac{b_2}{a_2\gamma_2}\left[A_2^*sh\left(\beta_m^*z_2^*\right) + B_2^*ch\left(\beta_m^*z_2^*\right)\right] - \frac{b_3}{a_3\gamma_3}\left[A_2^*sh\left(\beta_m^*z_3^*\right) + B_2^*ch\left(\beta_m^*z_3^*\right)\right]\right\}\\
&+ \sum_{m=1}^{\infty}\sum_{n=1}^{\infty}A_0^*DDJ_0\left(\beta_m^*r^*\right)\left[\frac{b_3}{a_3\gamma_3}\cos\sqrt{\left(\lambda_n^{*2} - \beta_m^{*2}\right)}z_3^* - \frac{b_4}{a_4}\cos\sqrt{\left(\lambda_n^{*2} - \beta_m^{*2}\right)}z_4^*\right] - \Theta_1^*,
\end{aligned} \tag{18}$$

$$\begin{aligned}
\sigma_{zr}^* = \frac{\sigma_{zr}}{G} &= -\sum_{m=1}^{\infty}\beta_m^{*2}J_1\left(\beta_m^*r^*\right)\left[A_1^*ch\left(\beta_m^*z_1^*\right) + B_1^*sh\left(\beta_m^*z_1^*\right) + A_2^*ch\left(\beta_m^*z_2^*\right) + B_2^*sh\left(\beta_m^*z_2^*\right) - A_1^*ch\left(\beta_m^*z_3^*\right)\right.\\
&\left. - B_1^*sh\left(\beta_m^*z_3^*\right) - A_2^*ch\left(\beta_m^*z_3^*\right) - B_2^*sh\left(\beta_m^*z_3^*\right)\right]\\
&- \sum_{m=1}^{\infty}\sum_{n=1}^{\infty}A_0^*DD\frac{\beta_m^*J_1\left(\beta_m^*r^*\right)}{\sqrt{\left(\lambda_n^{*2} - \beta_m^{*2}\right)}}\left[\sin\sqrt{\left(\lambda_n^{*2} - \beta_m^{*2}\right)}z_3^* - \sin\sqrt{\left(\lambda_n^{*2} - \beta_m^{*2}\right)}z_4^*\right],
\end{aligned} \tag{19}$$

$$\sigma_{rr}^{*}=\frac{\sigma_{rr}}{G}=\sum_{m=1}^{\infty}\beta_m^{*2}J_0(\beta_m^{*}r^{*})\left\{\frac{d_1}{a_1\gamma_1}\left[A_1^{*}sh(\beta_m^{*}z_1^{*})+B_1^{*}ch(\beta_m^{*}z_1^{*})\right]+\frac{d_2}{a_2\gamma_2}\left[A_2^{*}sh(\beta_m^{*}z_2^{*})+B_2^{*}ch(\beta_m^{*}z_2^{*})\right]\right.$$
$$\left.-\frac{d_3}{a_3\gamma_3}\left[A_1^{*}sh(\beta_m^{*}z_3^{*})+B_1^{*}ch(\beta_m^{*}z_3^{*})+A_2^{*}sh(\beta_m^{*}z_3^{*})+B_2^{*}ch(\beta_m^{*}z_3^{*})\right]\right\}$$
$$+\sum_{m=1}^{\infty}\sum_{n=1}^{\infty}A_0^{*}DDJ_0(\beta_m^{*}r^{*})\left[\frac{d_3}{a_3\gamma_3}\cos\sqrt{\left(\lambda_n^{*2}-\beta_m^{*2}\right)}z_3^{*}-\frac{d_4}{a_4}\cos\sqrt{\left(\lambda_n^{*2}-\beta_m^{*2}\right)}z_4^{*}\right]$$
$$-\frac{c_{12}-c_{11}}{r^{*}}\left\langle\sum_{m=1}^{\infty}\beta_m^{*}J_1(\beta_m^{*}r^{*})\left\{\frac{\gamma_1}{a_1}\left[A_1^{*}sh(\beta_m^{*}z_1^{*})+B_1^{*}ch(\beta_m^{*}z_1^{*})\right]+\frac{\gamma_2}{a_2}\left[A_2^{*}sh(\beta_m^{*}z_2^{*})+B_2^{*}ch(\beta_m^{*}z_2^{*})\right]\right.\right.$$
$$\left.-\frac{\gamma_3}{a_3}\left[A_1^{*}sh(\beta_m^{*}z_3^{*})+B_1^{*}ch(\beta_m^{*}z_3^{*})+A_2^{*}sh(\beta_m^{*}z_3^{*})+B_2^{*}ch(\beta_m^{*}z_3^{*})\right]\right\}$$
$$\left.-\sum_{m=1}^{\infty}\sum_{n=1}^{\infty}\frac{A_0^{*}DD}{\left(\lambda_n^{*2}-\beta_m^{*2}\right)}\left[\frac{\gamma_3}{a_3}\cos\sqrt{\left(\lambda_n^{*2}-\beta_m^{*2}\right)}z_3^{*}-\frac{1}{a_4}\cos\sqrt{\left(\lambda_n^{*2}-\beta_m^{*2}\right)}z_4^{*}\right]\right\rangle-\frac{\lambda_{11}}{\lambda_{33}}\Theta_1^{*},\tag{20}$$

$$\sigma_{\theta\theta}^{*}=\frac{\sigma_{\theta\theta}}{G}=\sum_{m=1}^{\infty}\beta_m^{*2}J_0(\beta_m^{*}r^{*})\left\{\frac{f_1}{a_1\gamma_1}\left[A_1^{*}sh(\beta_m^{*}z_1^{*})+B_1^{*}ch(\beta_m^{*}z_1^{*})\right]+\frac{f_2}{a_2\gamma_2}\left[A_2^{*}sh(\beta_m^{*}z_2^{*})+B_2^{*}ch(\beta_m^{*}z_2^{*})\right]\right.$$
$$\left.-\frac{f_3}{a_3\gamma_3}\left[A_1^{*}sh(\beta_m^{*}z_3^{*})+B_1^{*}ch(\beta_m^{*}z_3^{*})+A_2^{*}sh(\beta_m^{*}z_3^{*})+B_2^{*}ch(\beta_m^{*}z_3^{*})\right]\right\}$$
$$+\sum_{m=1}^{\infty}\sum_{n=1}^{\infty}A_0^{*}DDJ_0(\beta_m^{*}r^{*})\left[\frac{f_3}{a_3\gamma_3}\cos\sqrt{\left(\lambda_n^{*2}-\beta_m^{*2}\right)}z_3^{*}-\frac{f_4}{a_4}\cos\sqrt{\left(\lambda_n^{*2}-\beta_m^{*2}\right)}z_4^{*}\right]$$
$$+\frac{c_{12}-c_{11}}{r^{*}}\left\langle\sum_{m=1}^{\infty}\beta_m^{*}J_1(\beta_m^{*}r^{*})\left\{\frac{\gamma_1}{a_1}\left[A_1^{*}sh(\beta_m^{*}z_1^{*})+B_1^{*}ch(\beta_m^{*}z_1^{*})\right]+\frac{\gamma_2}{a_2}\left[A_2^{*}sh(\beta_m^{*}z_2^{*})+B_2^{*}ch(\beta_m^{*}z_2^{*})\right]\right.\right.$$
$$\left.-\frac{\gamma_3}{a_3}\left[A_1^{*}sh(\beta_m^{*}z_3^{*})+B_1^{*}ch(\beta_m^{*}z_3^{*})+A_2^{*}sh(\beta_m^{*}z_3^{*})+B_2^{*}ch(\beta_m^{*}z_3^{*})\right]\right\}$$
$$\left.-\sum_{m=1}^{\infty}\sum_{n=1}^{\infty}\frac{A_0^{*}DD}{\left(\lambda_n^{*2}-\beta_m^{*2}\right)}\left[\frac{\gamma_3}{a_3}\cos\sqrt{\left(\lambda_n^{*2}-\beta_m^{*2}\right)}z_3^{*}-\frac{1}{a_4}\cos\sqrt{\left(\lambda_n^{*2}-\beta_m^{*2}\right)}z_4^{*}\right]\right\rangle-\frac{\lambda_{11}}{\lambda_{33}}\Theta_1^{*}.\tag{21}$$

When the Eqs. (12) and (15) are substituted into Eq. (11), the dimensionless formulation of displacement fields are obtained as,

$$w^{*}=\frac{a_1}{Gd}w=a_1\sum_{m=1}^{\infty}\beta_m^{*}J_0(\beta_m^{*}r^{*})\left\{\frac{l_{11}}{a_1}\left[A_1^{*}ch(\beta_m^{*}z_1^{*})+B_1^{*}sh(\beta_m^{*}z_1^{*})\right]-\frac{l_{13}}{a_3}\left[A_1^{*}ch(\beta_m^{*}z_3^{*})+B_1^{*}sh(\beta_m^{*}z_3^{*})\right]\right.$$
$$\left.+\frac{l_{12}}{a_2}\left[A_2^{*}ch(\beta_m^{*}z_2^{*})+B_2^{*}sh(\beta_m^{*}z_2^{*})\right]-\frac{l_{13}}{a_3}\left[A_2^{*}ch(\beta_m^{*}z_3^{*})+B_2^{*}sh(\beta_m^{*}z_3^{*})\right]\right\}$$
$$+a_1\sum_{m=1}^{\infty}\sum_{n=1}^{\infty}A_0^{*}DD\frac{J_0(\beta_m^{*}r^{*})}{\sqrt{\left(\lambda_n^{*2}-\beta_m^{*2}\right)}}\left[\frac{l_{13}}{a_3}\sin\sqrt{\left(\lambda_n^{*2}-\beta_m^{*2}\right)}z_3^{*}-\frac{l_{14}}{a_4}\sin\sqrt{\left(\lambda_n^{*2}-\beta_m^{*2}\right)}z_4^{*}\right],\tag{22}$$

$$u^* = \frac{a_1}{Gd}u = -a_1\sum_{m=1}^{\infty}\beta_m^* J_1(\beta_m^* r^*)\left\{\frac{\gamma_1}{a_1}\left[A_1^* sh(\beta_m^* z_1^*) + B_1^* ch(\beta_m^* z_1^*)\right] - \frac{\gamma_3}{a_3}\left[A_1^* sh(\beta_m^* z_3^*) + B_1^* ch(\beta_m^* z_3^*)\right]\right.$$
$$\left. + \frac{\gamma_2}{a_2}\left[A_2^* sh(\beta_m^* z_2^*) + B_2^* ch(\beta_m^* z_2^*)\right] - \frac{\gamma_3}{a_3}\left[A_2^* sh(\beta_m^* z_3^*) + B_2^* ch(\beta_m^* z_3^*)\right]\right\}$$
$$+ a_1\sum_{m=1}^{\infty}\sum_{n=1}^{\infty}A_0^* DD\frac{\beta_m^* J_1(\beta_m^* r^*)}{\left(\lambda_n^{*2} - \beta_m^{*2}\right)}\left[\frac{\gamma_3}{a_3}\cos\sqrt{\left(\lambda_n^{*2} - \beta_m^{*2}\right)}z_3^* - \frac{1}{a_4}\cos\sqrt{\left(\lambda_n^{*2} - \beta_m^{*2}\right)}z_4^*\right]. \quad (23)$$

When the Eqs. (12) and (15) are substituted into the latter two formulas of Eq. (16), the dimensionless formulation of electric displacement fields can be obtained and they are written in the following

$$D_z^* = \frac{D_z}{F} = \frac{\lambda_{33}}{p_3}\left\langle\sum_{m=1}^{\infty}\beta_m^{*2} J_0(\beta_m^* r^*)\left\{\frac{c_1}{a_1\gamma_1}\left[A_1^* sh(\beta_m^* z_1^*) + B_1^* ch(\beta_m^* z_1^*)\right] + \frac{c_2}{a_2\gamma_2}\left[A_2^* sh(\beta_m^* z_2^*) + B_2^* ch(\beta_m^* z_2^*)\right]\right.\right.$$
$$\left. - \frac{c_3}{a_3\gamma_3}\left[A_1^* sh(\beta_m^* z_3^*) + B_1^* ch(\beta_m^* z_3^*) + A_2^* sh(\beta_m^* z_3^*) + B_2^* ch(\beta_m^* z_3^*)\right]\right\}$$
$$\left. + \sum_{m=1}^{\infty}\sum_{n=1}^{\infty}A_0^* DDJ_0(\beta_m^* r^*)\left[\frac{c_3}{a_3\gamma_3}\cos\sqrt{\left(\lambda_n^{*2} - \beta_m^{*2}\right)}z_3^* - \frac{c_4}{a_4}\cos\sqrt{\left(\lambda_n^{*2} - \beta_m^{*2}\right)}z_4^*\right]\right\rangle + \Theta_1^*, \quad (24)$$

$$D_r^* = \frac{D_r}{F} = -\sum_{m=1}^{\infty}\beta_m^{*2} J_1(\beta_m^* r^*)\left\{\frac{g_1}{a_1}\left[A_1^* ch(\beta_m^* z_1^*) + B_1^* sh(\beta_m^* z_1^*)\right] + \frac{g_2}{a_2}\left[A_2^* ch(\beta_m^* z_2^*) + B_2^* sh(\beta_m^* z_2^*)\right]\right.$$
$$\left. - \frac{g_3}{a_3}\left[A_1^* ch(\beta_m^* z_3^*) + B_1^* sh(\beta_m^* z_3^*) + A_2^* ch(\beta_m^* z_3^*) + B_2^* sh(\beta_m^* z_3^*)\right]\right\}$$
$$- \sum_{m=1}^{\infty}\sum_{n=1}^{\infty}A_0^* DD\frac{\beta_m^* J_1(\beta_m^* r^*)}{\sqrt{\left(\lambda_n^{*2} - \beta_m^{*2}\right)}}\left[\frac{g_3}{a_3}\sin\sqrt{\left(\lambda_n^{*2} - \beta_m^{*2}\right)}z_3^* - \frac{g_4}{a_4}\sin\sqrt{\left(\lambda_n^{*2} - \beta_m^{*2}\right)}z_4^*\right] + \frac{p_1}{p_3}\Theta_1^*. \quad (25)$$

The corresponding factors γ_i, a_i, b_i, c_i, d_i, f_i, g_i, l_{ji}, $i = 1, 2, 3, 4$, $j = 1, 2$ in the above equations are defined. The unknown functions $A_1^*, B_1^*, A_2^*, B_2^*$ can be determined by the boundary conditions of forces, displacements and electric displacements. The details will be given in the following section.

3. Calculated results and discussion

The above theoretical model is used to study the thermopiezoelectric response of PZT-6B deposited on MgO(1 0 0) substrate induced by a continuous laser beam heating. The results will be given as detail as possible. The geometrical parameters are given in Fig. 1 with the radius of sample $r_0 = 15$ mm, the thickness of thin film $h = 2$ μm and the thickness of substrate $H = 2$ mm.

3.1. Material parameters

As we know, due to the size effect, the material parameters of thin film should be different from those of bulk materials. However, the material parameters of PZT thin film are so few that they cannot be found in the references. In the study, the material parameters of bulk PZT are adopted as the parameters of PZT thin film. On the other hand, the physical parameters should be all temperature dependent. However, the temperature dependent parameters cannot easily be found in the references. Therefore, the physical parameters are all not dependent on temperature in the present investigation. Thermal physical parameters of bulk PZT, such as the density, specific heat, thermal conductivity and thermal expansion coefficient, are

Table 1
Thermal physical parameters

	Density (10^3 kg/m^3)	Specific heat (J/kg °C)	Thermal conductivity (W/m °C)	Thermal diffusivity (m^2/s)	Thermal expansion coefficient (10^{-6} K^{-1})
PZT-6B	7.6	420	1.2	3.76×10^{-7}	7
MgO	3.58	976	710	2.03×10^{-4}	

Table 2
Mechanical physical parameters (PZT-6B)

Elastic coefficients (10^{10} N m^{-2})					Piezoelectric coefficients (C m^{-2})			Dielectric coefficients (10^{-10} F m^{-1})		Pyroelectric coefficients (10^{-4} C K^{-1} m^{-2})		Thermal modulus (10^6 N K^{-1} m^{-2})	
c_{11}	c_{33}	c_{44}	c_{13}	c_{12}	e_{15}	e_{31}	e_{33}	ϵ_{11}	ϵ_{33}	p_1	p_3	λ_{11}	λ_{33}
16.8	16.3	2.71	6.0	6.0	4.6	−0.9	7.1	36.0	34.0	0	3.7	2.016	1.981

Table 3
Evolution of related constants for PZT-6B

$\mu_i = [3.7326, 0.2264, 0.9719]$	$\gamma_i = [1.9320, 0.4759, 0.9859]$
$l_{1j} = [6.5507, 0.1268, -0.1620, -0.1774]$	$l_{2j} = [0.7948, -0.0027, 4.0620, 3.7357]$
$a_i = [24.1184, 3.0411, 20.9564, 19.4133]$	$b_i = [90.0240, 0.6886, 20.9564, 17.6316]$
$c_i = [22.8465, 1.1957, -138.3848, -127.3722]$	$d_i = [-24.1184, -3.0411, -20.9564, -21.2265]$
$f_i = [16.1934, -0.5956, -10.4594, -10.4265]$	$g_i = [6.1208, 5.2804, -142.3787, -130.7000]$

taken from the literatures (Setter and Colla, 1993; Xu, 1991). The thermal diffusivity coefficient can be calculated and the results for PZT thin film and MgO substrate are listed in Table 1. For a transversely isotropic thermopiezoelectric body, the number of independent physical constants is 14, with 5 in elastic coefficients, 2 in dielectric coefficients, 3 in piezoelectric coefficients, 2 in pyroelectric coefficients and 2 in thermal modulus. The coefficients are taken from Shang et al. (1996) and Wang and Zheng (1995) and they are listed in Table 2. The thermal modulus can be calculated from the stress–strain relation and the strain–displacement relation in Eq. (10) and the results are also listed in Table 2. Other constants defined are listed in Table 3.

3.2. Boundary conditions

According to the mode assumptions, the boundary conditions on the outer surface and continuous condition at interface for traction, electric and displacement can be written in the following,

$$\sigma^*_{zz}|_{z^*=0} = 0; \quad D^*_z|_{z^*=0} = 0; \quad D^*_z\Big|_{z^*=h\sqrt{K_c}} = 0; \quad w^*\Big|_{z^*=h\sqrt{K_c}} = 0. \tag{26}$$

In this case, the functions $A^*_1, B^*_1, A^*_2, B^*_2$ can be determined from the above equations. If the expressions for stress, electric displacement and displacement are substituted into the above equations, linear algebra equations for variables $A^*_1, B^*_1, A^*_2, B^*_2$ can be obtained. It is natural that the linear algebra equations can easily be solved.

3.3. Temperature variation with r, z and t

Temperature fields due to a pulsed laser irradiation are primarily controlled by the temporal pulsed profile and the radial intensity distribution. The temporal pulsed profile expresses distribution of pulse

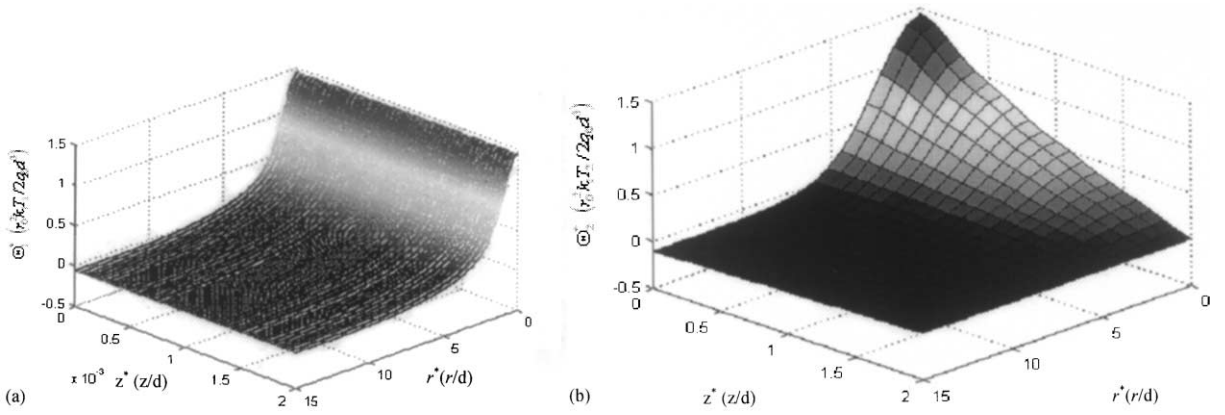

Fig. 3. Steady-state spatial distribution of temperature fields at selected time $t^* = 1$: (a) PZT thin film, (b) MgO substrate.

energy in time and the radial intensity distribution is determined by the characteristic beam radius d and the maximum incident flux for Gaussian source q_0 The two-dimensional spatial distributions of temperature fields in the thin film PZT and MgO(1 0 0) substrate at $t^* = 1$ are shown in Fig. 3(a) and (b), respectively. It is seen that the temperature is constant in the thin film along thickness direction. The temperature in the center is much higher than that in the outer region of laser beam. However, the characteristic of temperature in substrate is different from that in thin film. It is seen that the temperature in the center and at the interface is much higher than that in other places. An example for temperature can be obtained according to the results shown in Fig. 3 and the definition of dimensionless variables in expressions (7). If the duration of continuous Gaussian source is taken as 2.66 s, the power density is taken as $q_0 = 400$ W/cm^2 and the characteristic beam radius is taken as $d = 2$ mm, the highest temperature in thin film is 391 °C and it is below the Curie temperature 490 °C (Setter and Colla, 1993). This means that the thin film will not have phase transformation in this case.

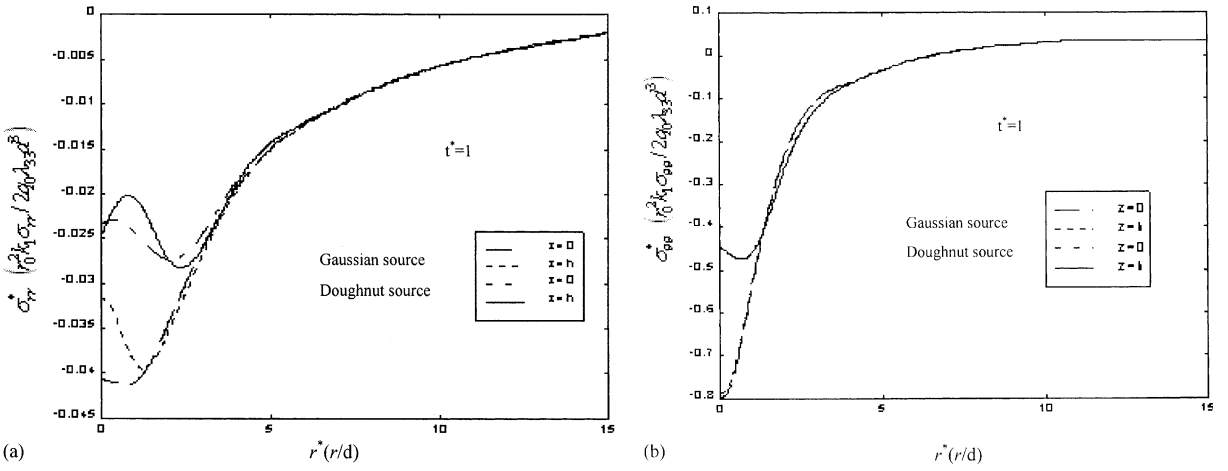

Fig. 4. Steady-state variation of radial stress σ^*_{rr} and circumferential stress $\sigma^*_{\theta\theta}$ in r-direction with different z at time $t^* = 1$: (a) σ^*_{rr} for $f = 0$ and $f = 1$, (b) $\sigma^*_{\theta\theta}$ for $f = 0$ and $f = 1$.

3.4. Thermal stresses

3.4.1. Radial stresses σ^*_{rr} and circumferential stresses $\sigma^*_{\theta\theta}$

Fig. 4 shows the radial and circumferential stress variations with radial distance from axis on the surface and at interface. It shows that the radial stresses at any place are compressive. However, the case for circumferential stress is different. The circumferential stresses in the radiating region of laser beam are compressive and those in the outer region of laser beam radiation are tensile stress. Although the tensile circumferential stress in the outer region of laser beam radiation is low, the tensile stress may induce the PZT thin film to damage for the brittle materials. This means that the damage will not be induced by radial stress and the damage should be induced by circumferential stress. In many experiments about the thermal failure of materials, one observed that the cracks were in the form of radial cracks and the cracks were not in the form of circumferential cracks (Zhou et al., 1998). It is natural that the elements in the inner laser heating region will expand and the expansion will meet the "cooler" elements outside of the edge of the beam. The numerical results shown in Fig. 4 denote that the thermal failure characteristics for PZT thin film should be same with other materials induced by laser beam.

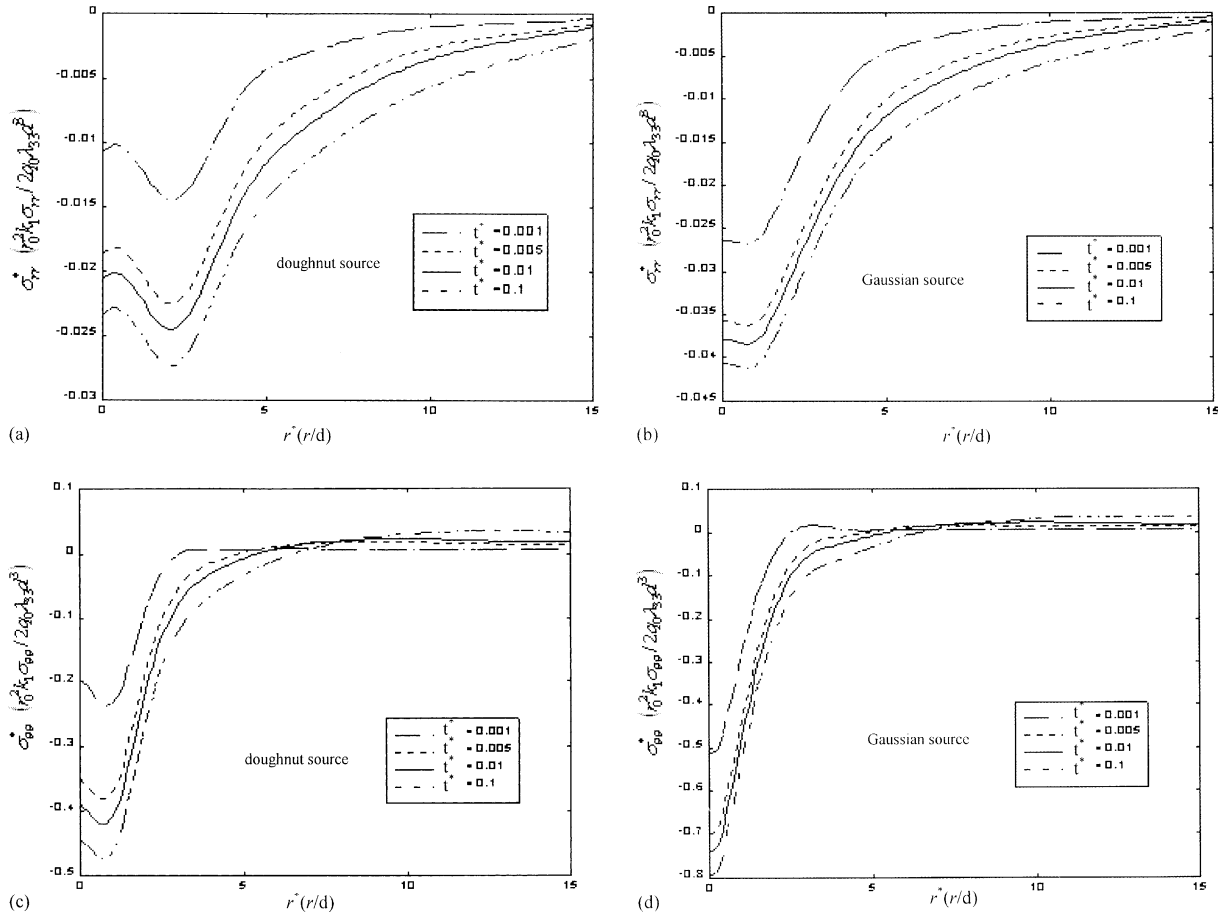

Fig. 5. Radial distribution of surface stresses at selected times ($t^* = 0.001, 0.005, 0.01, 0.1$): (a) σ^*_{rr} for $f = 0$, (b) σ^*_{rr} for $f = 1$, (c) $\sigma^*_{\theta\theta}$ for $f = 0$, (d) $\sigma^*_{\theta\theta}$ for $f = 1$.

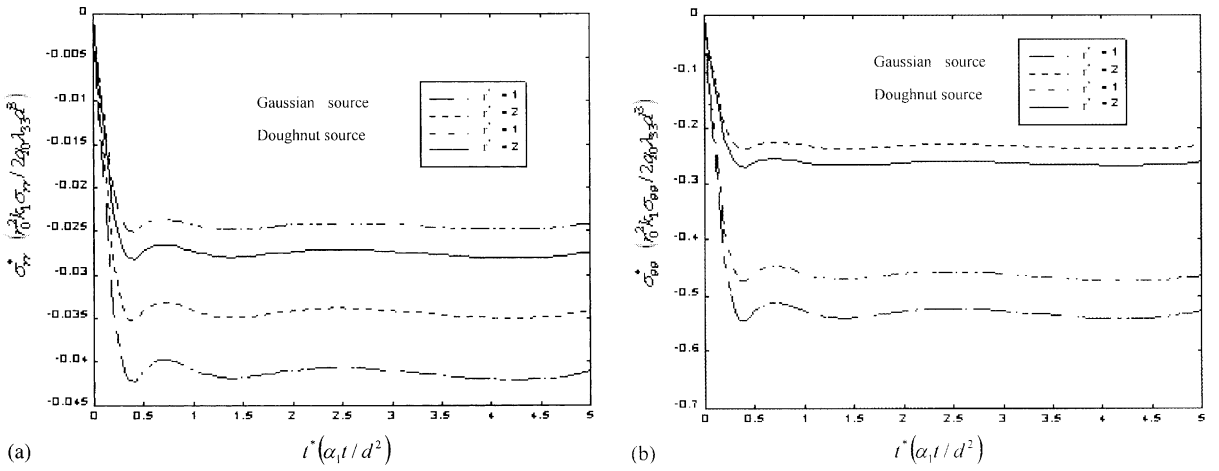

Fig. 6. Evolution of surface stresses at selected radial positions: (a) σ^*_{rr} for $f = 0$ and $f = 1$, (b) $\sigma^*_{\theta\theta}$ for $f = 0$ and $f = 1$.

It is found that the largest compressive stress is in the peak place of laser beam both for Gaussian and doughnut laser beam. On the other hand, the largest compressive stresses are on the surface of thin film and near the edge of laser beam.

Fig. 5 shows the spatial distribution of stresses on the surface at different time. Under a certain stationary source, the maximum compressive stress $\sigma^*_{\theta\theta}$ is larger than σ^*_{rr}. This means that the interface crack is possibly generated and propagated due to the buckling of the thin film and the buckling is induced by the compressive circumferential stress. Generally, the stress induced by Gaussian laser beam is larger than that induced by doughnut laser beam. Figs. 5 and 6 show that the variations of radial and circumferential stresses with time are rapid at the beginning of laser heating, however, when the non-dimensional time t^*_0 is larger than 0.3–0.45 the variation becomes more and more smooth. The variations of stress with the thickness of thin film are shown in Fig. 7, where the laser beam is Guassian stationary source $f = 1$ and the stress is in different places with $r^* = 0.1$ and 1 and the time is $t^* = 0.001$, 0.005, 0.01 and 0.1. It is easy to see that the variations of radial stress described in Fig. 7(a) and (b) are consistent with the distribution of radial stresses described by Fig. 4(a). Comparing Fig. 7(c), (d) and Fig. 4(b), we have the conclusion that the circumferential stress is not dependent on the thickness of thin film.

3.4.2. Normal stress σ^*_{zz} and tangent stress σ^*_{zr}

Observing Fig. 8, we can obtain the results as in the following. (1) The radial and circumferential stresses are much larger than the normal and tangent stress. (2) The normal and tangent stresses at interface vary rapidly during very short time $t^*_0 < 0.001$ and after non-dimensional time 0.001, they trend to a stable value. (3) The stress within laser beam radiation region is much larger than that in other place. The stress in the outer region of laser beam radiation region is almost zero. When the laser beam is continuous Gaussian source and the duration is 2.66 s, the maximum circumferential, radial, normal and tangent stresses at interface are about -355.06, -18.94, -0.59 and -0.32 MPa, respectively. With the increment of depth of thin film, the normal and tangent stress increase as shown in Fig. 9. However, the variations of normal and tangent stress with the depth of thin film are small. In the above section, the circumferential, radial stresses induced by Gaussian source are larger than those induced by doughnut source. However, one can see another interesting phenomenon shown in Fig. 9 and the phenomenon is that the normal and tangent stresses induced by doughnut source are larger than those induced by the Gaussian laser beam.

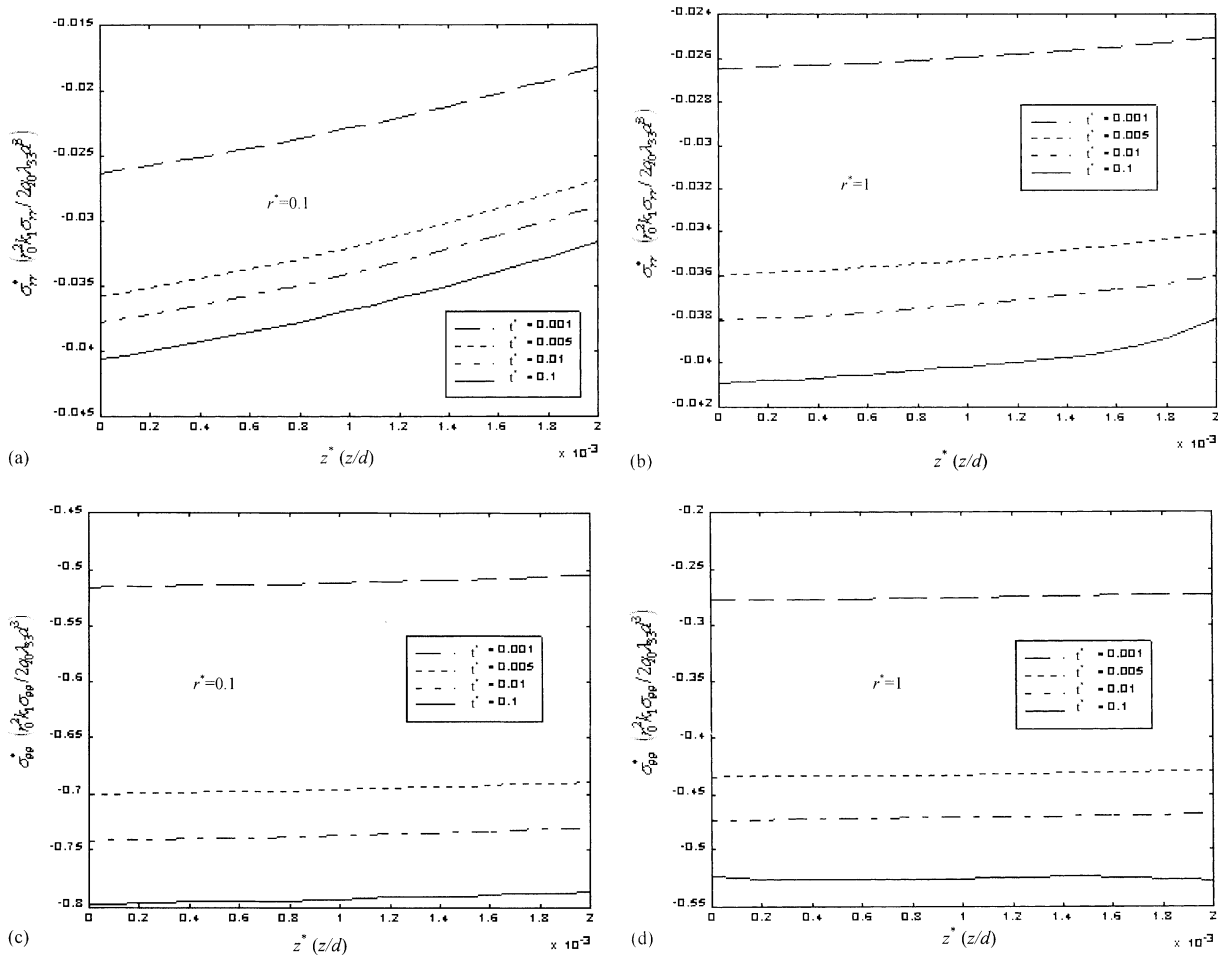

Fig. 7. Axial variation of stress fields at selected times ($t^* = 0.001, 0.005, 0.01, 0.1$) for Gaussian source: (a) σ^*_{rr} for $r^* = 0.1$, (b) σ^*_{rr} for $r^* = 1$, (c) $\sigma^*_{\theta\theta}$ for $r^* = 0.1$, (d) $\sigma^*_{\theta\theta}$ for $r^* = 1$.

3.5. Displacement u^* and w^*

The displacements u^* and w^* are shown in Fig. 10. It is found that the displacement in r-direction is larger two orders of magnitude than that in z-direction. The maximum vertical displacement w^* is induced by the doughnut source and the maximum horizontal displacement u^* is induced by Gaussian source. The vertical displacement w^* can be evaluated by Eq. (22) and it is 10^{-2}–10^{-4} μm. The displacement is much less than the thickness of the thin film (1 μm). For example, the maximum horizontal displacement u^* for Gaussian source with the duration of 2.66 s is 2.61 μm at the interface, however, the maximum vertical displacement w^* for doughnut source with the duration of 2.66 s is −16.72 nm on the surface. This means that the displacement in vertical direction is much smaller than that in the horizontal direction. Fig. 11 shows that the variations of displacements with time are rapid at the beginning of laser heating, however, when the non-dimensional time t^*_0 is larger than 0.3–0.45 the variation becomes more and more smooth.

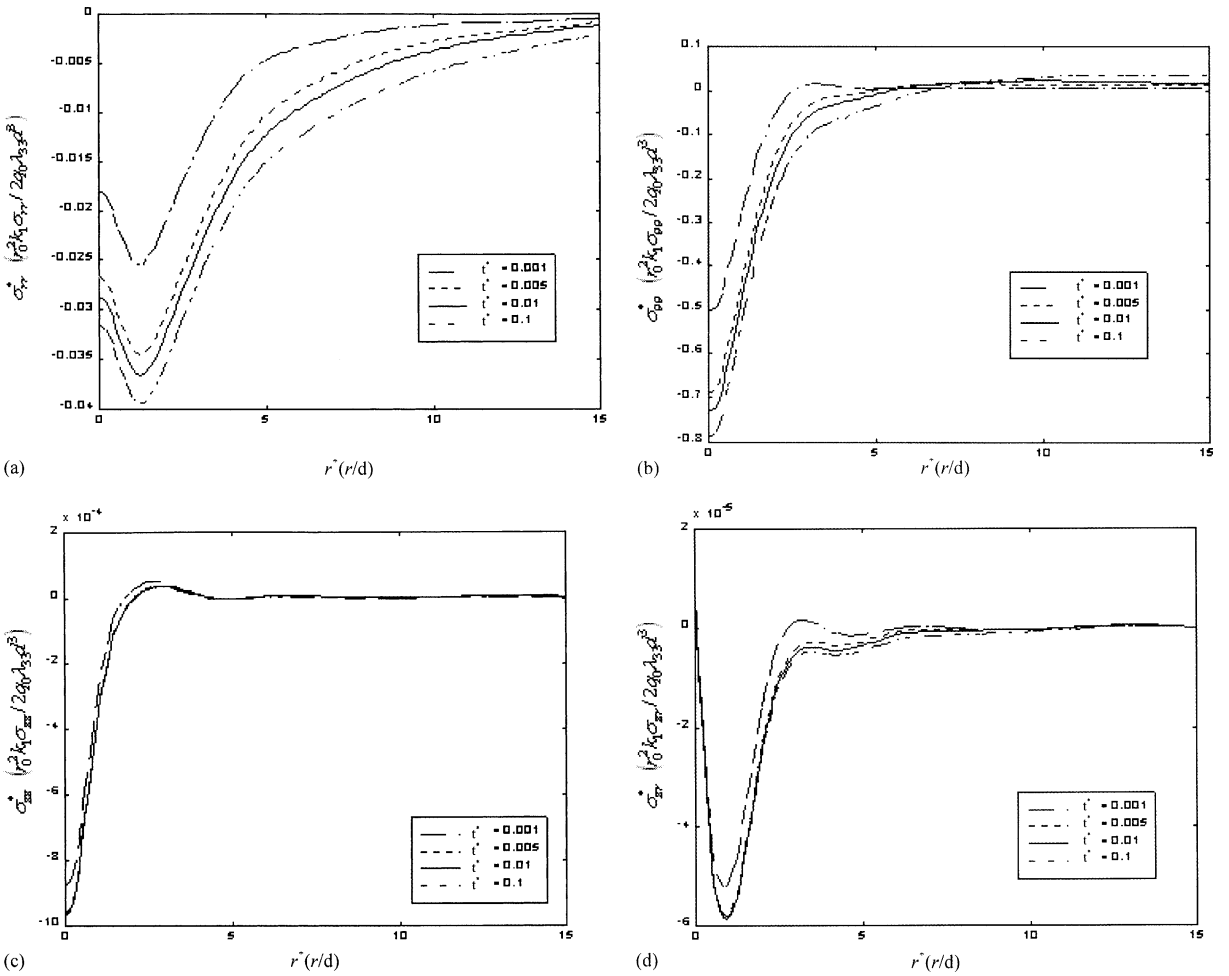

Fig. 8. Radial distribution of interface stress at selected times ($t^* = 0.001, 0.005, 0.01, 0.1$) for Gaussian source: (a) σ^*_{rr}, (b) $\sigma^*_{\theta\theta}$, (c) σ^*_{zz}, (d) σ^*_{zr}.

3.6. Electric displacement D^*_z and D^*_r

Fig. 12 shows the steady-state variation of horizontal electric displacement D^*_r and vertical electric displacement D^*_z with distance from axis at selected depths $z = h/2$ and time $t^* = 1$. Comparing D^*_z and D^*_r variation with the distance from the center of laser beam at a certain time $t^* = 1$, one can see that the horizontal electric displacement D^*_r is much larger than that of vertical electric displacement D^*_z. On the other hand, the electric displacement D^*_r and D^*_z induced by doughnut source is much larger than those induced by the Gaussian source. Fig. 13 shows that the variations of electric displacements with time are rapid at the beginning of laser heating, however, when the non-dimensional time t^*_0 is larger than 0.3–0.45 the variation becomes more and more smooth. Fig. 14 shows the axial variation of electric displacement fields at selected times ($t^* = 0.001, 0.005, 0.01, 0.1$) with the Gaussian source. When the duration is 2.66 s for Gaussian laser beam, the maximum horizontal and vertical electric displacements with $z = h/2$ are, respectively, 0.91 and -1.16×10^{-3} C/m^2.

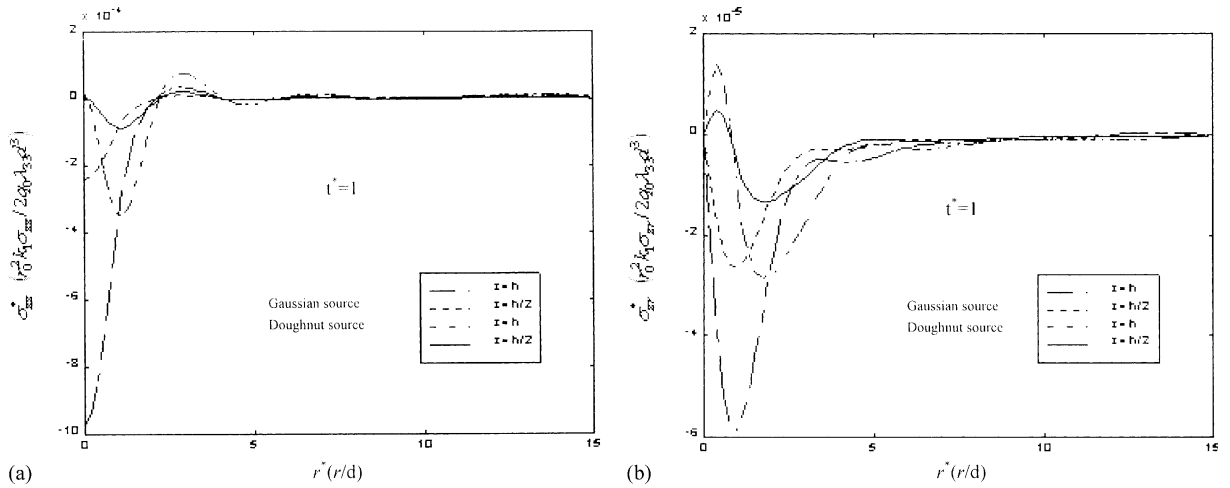

Fig. 9. Steady-state variation of normal stress and shear stress in r-direction with different z at time $t^* = 1$: (a) σ^*_{zz} for $f = 0$ and $f = 1$, (b) σ^*_{zr} for $f = 0$ and $f = 1$.

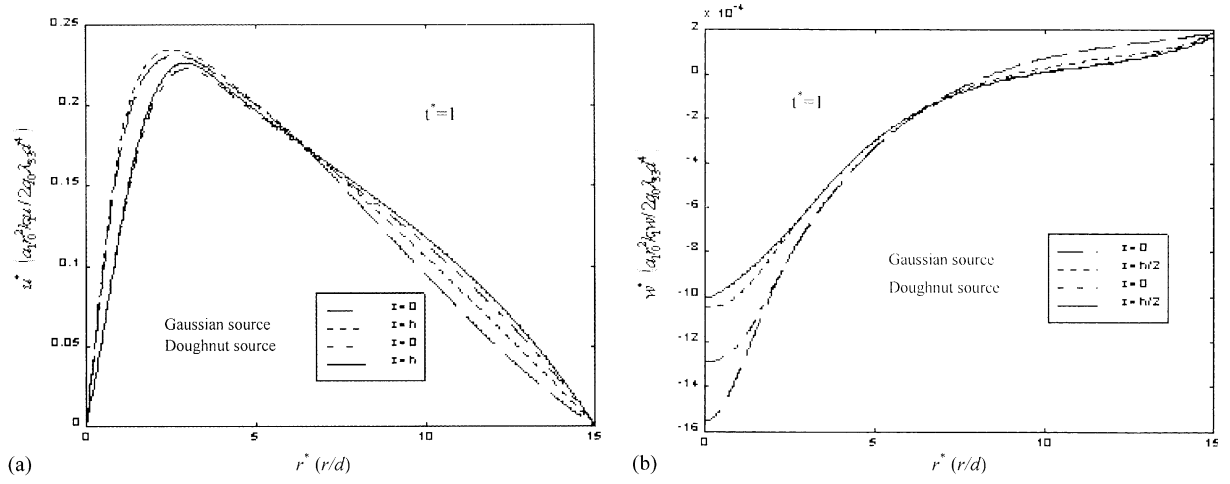

Fig. 10. Steady-state variation of horizontal displacement u^* and vertical displacement w^* in r-direction with different z and time: (a) u^*, (b) w^*.

4. Concluding remarks

In the present investigation, a theoretical model is proposed to study the thermopiezoelectric response of piezoelectric thin films induced by laser beam heating. The temperature, stress, displacement and electric displacement fields of PZT-6B thin film are analytically obtained. The numerical results are also obtained and the characteristics of fields are mainly discussed. The main conclusions can be listed as in the following.

(1) Temperature field is primarily controlled by the temporal and spatial pulsed profile. Various temperature fields can be obtained when the power density and the characteristic radius of laser beam are adjusted.

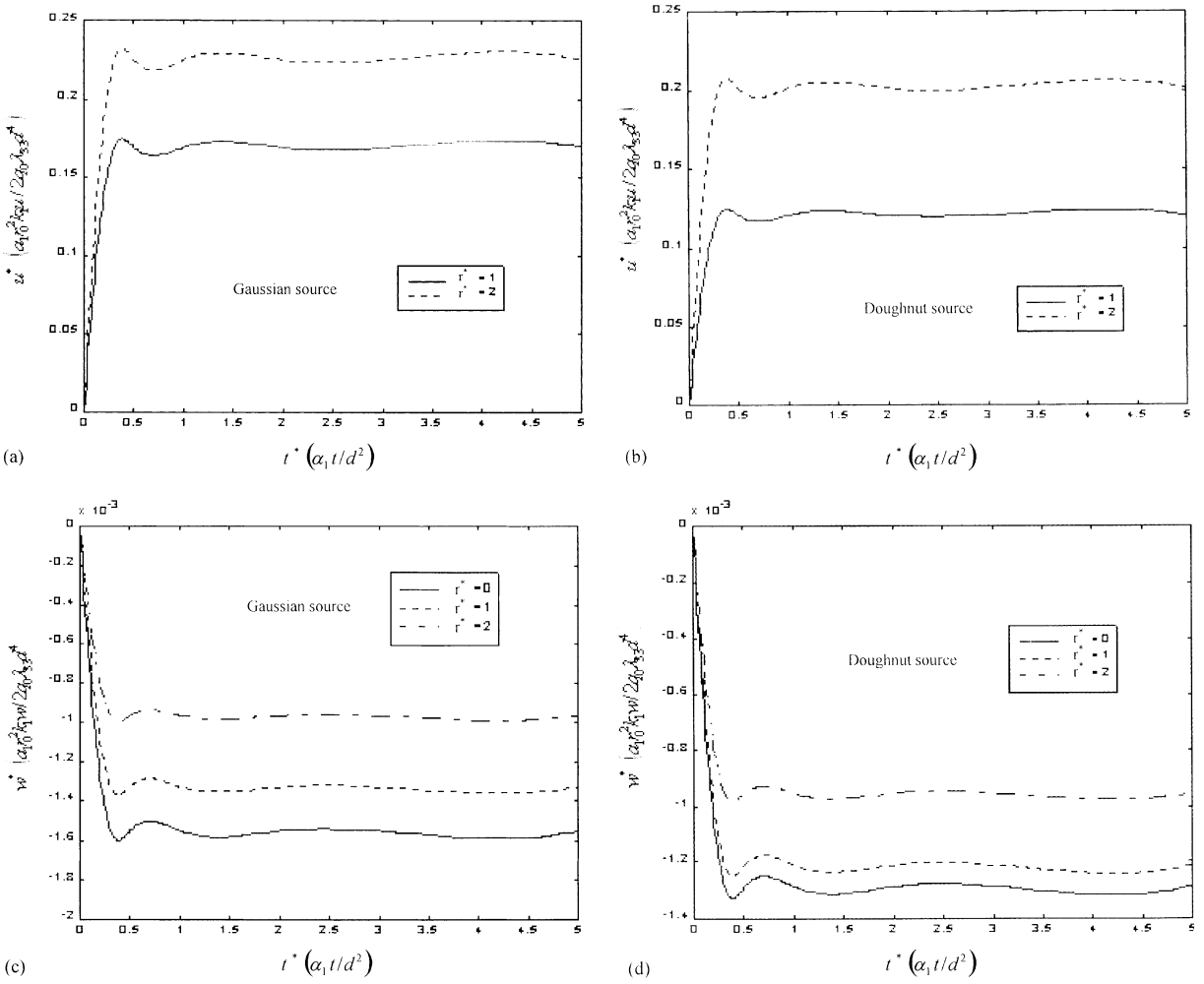

Fig. 11. Evolution of surface displacements at selected radial positions: (a) u^* for $f = 1$, (b) u^* for $f = 0$, (c) w^* for $f = 1$, (d) w^* for $f = 0$.

(2) The radial and circumferential stresses are almost not dependent on the depth, i.e. z. It is due to the fact that the thickness of film is much thinner than the substrate. Comparing doughnut laser beam, the Gaussian laser beam will induce a higher radial and circumferential stresses. However, the doughnut laser beam will induce a higher normal and tangent stresses. The stresses in the laser beam irradiated region are much larger than those in the other places. The variations of stresses with time are rapid at the beginning of laser heating, however, when the non-dimensional time t_0^* is larger than 0.3–0.45 the variation becomes more and more smooth.

(3) The maximum vertical displacement w^* is induced by the doughnut source and the maximum horizontal displacement u^* is induced by Gaussian source. The displacement in vertical direction is much smaller than that in the horizontal direction.

(4) The horizontal electric displacement D_r^* is much larger than that of vertical electric displacement D_z^*.

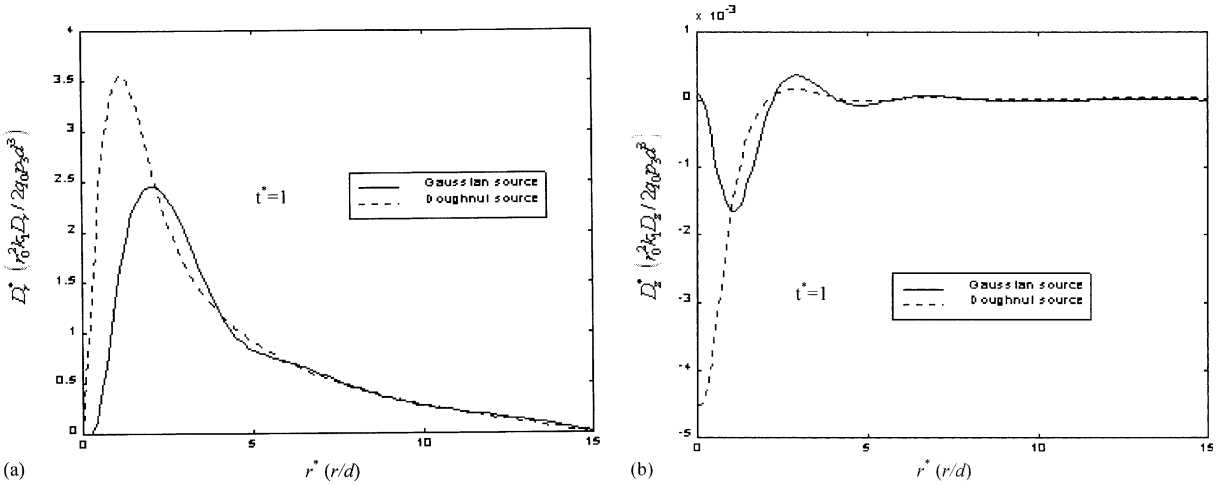

Fig. 12. Steady-state variation of radial electric-displacement D_r^* and vertical electric displacement D_z^* in r-direction at selected depths $z = h/2$ and time $t^* = 1$: (a) D_r^* for $f = 0$ and $f = 1$, (b) D_z^* for $f = 0$ and $f = 1$.

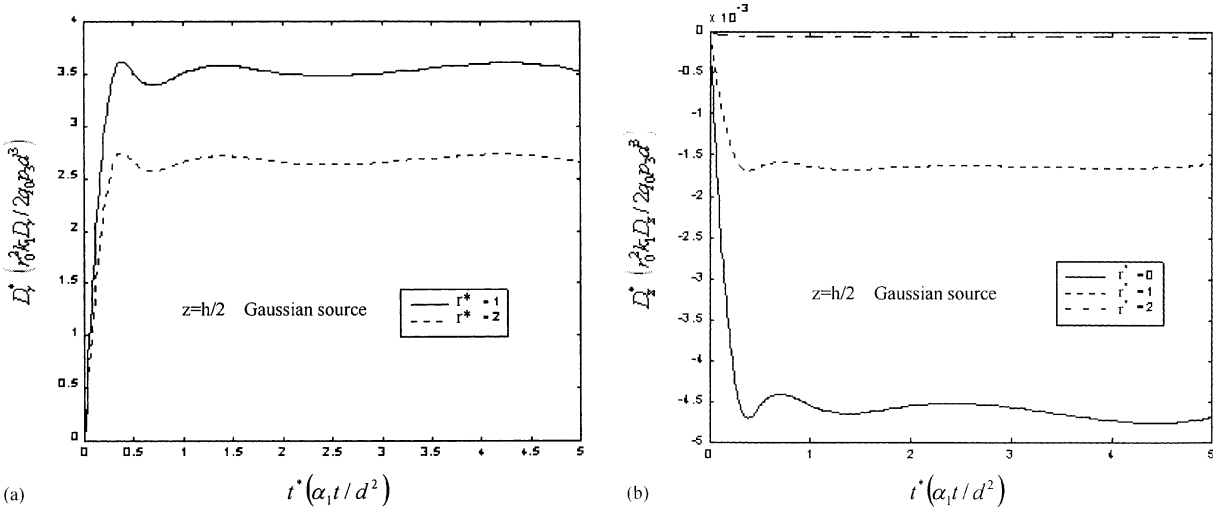

Fig. 13. Evolution of electric displacement field at $z = h/2$ and selected radial positions for Gaussian source: (a) D_r^*, (b) D_z^*.

Acknowledgement

The project was supported by the National Natural Science Foundation of China (10072052).

Appendix A

In this appendix, some coefficients and functions are listed. The coefficient $A_0(\beta_m, \lambda_n, t)$ for temperature fields can be written as

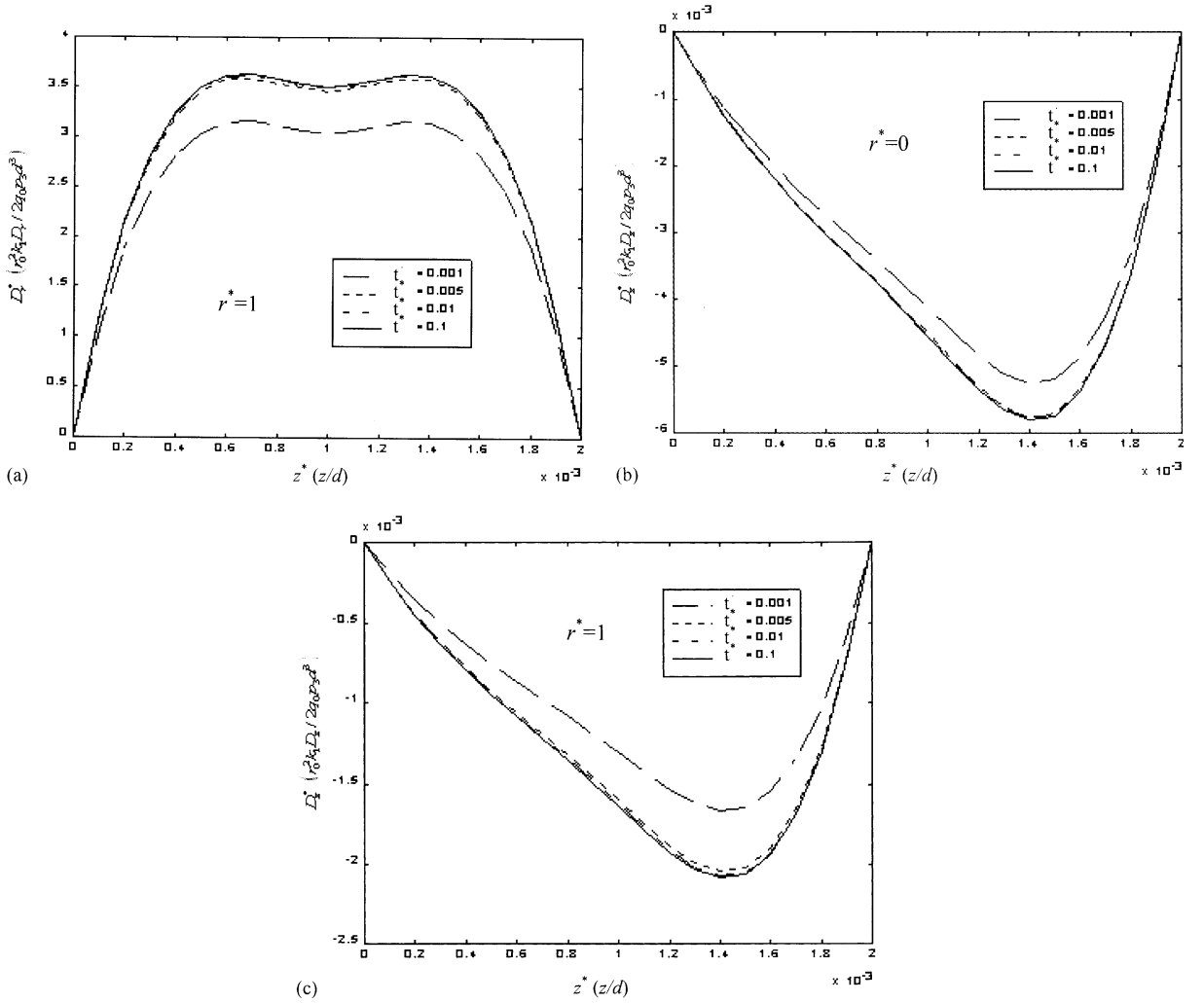

Fig. 14. Axial variation of electric displacement fields at selected times ($t^* = 0.001, 0.005, 0.01, 0.1$) for Gaussian source: (a) D_r^* for $r^* = 0$, (b) D_r^* for $r^* = 1$, (c) D_z^* for $r^* = 1$.

$$A_0(\beta_m, \lambda_n, t) = \frac{2\int_0^{r_0} J_0(\beta_m r) f_1(r, z, t) r \, \mathrm{d}r \int_{\tau=0}^{t} \mathrm{e}^{-\lambda_n^2(t-\tau)} \, \mathrm{d}\tau}{r_0^2 J_0^2(\beta_m r_0) N(\beta_m, \lambda_n)}. \tag{A.1}$$

The fundamental functions are given in the following:

$$R_0(\beta_m, r) = J_0(\beta_m r), \tag{A.2}$$

$$Z_{1,n}(\beta_m, \lambda_n, z) = \cos\sqrt{\left(\frac{\lambda_n^2}{\alpha_1} - \beta_m^2\right)} z, \tag{A.3}$$

$$Z_{2,n}(\beta_m,\lambda_n,z)=\cos\sqrt{\left(\frac{\lambda_n^2}{\alpha_1}-\beta_m^2\right)}h\cos\sqrt{\left(\frac{\lambda_n^2}{\alpha_2}-\beta_m^2\right)}(h-z)+\frac{k_1\sqrt{\left(\frac{\lambda_n^2}{\alpha_1}-\beta_m^2\right)}}{k_2\sqrt{\left(\frac{\lambda_n^2}{\alpha_2}-\beta_m^2\right)}}\times\sin\sqrt{\left(\frac{\lambda_n^2}{\alpha_1}-\beta_m^2\right)}h\sin\sqrt{\left(\frac{\lambda_n^2}{\alpha_2}-\beta_m^2\right)}(h-z). \tag{A.4}$$

The norms are written in the following:

$$\frac{1}{N(\beta_m)}=\frac{2}{r_0^2J_0^2(\beta_m r_0)}, \tag{A.5}$$

$$N(\beta_m,\lambda_n)=\rho_1c_{p1}\int_0^h\cos^2\left[\sqrt{\left(\frac{\lambda_n^2}{\alpha_1}-\beta_m^2\right)}z\right]\mathrm{d}z+\rho_2c_{p2}\int_h^H\left[\cos\sqrt{\left(\frac{\lambda_n^2}{\alpha_1}-\beta_m^2\right)}h\cos\sqrt{\left(\frac{\lambda_n^2}{\alpha_2}-\beta_m^2\right)}(h-z)+\frac{k_1\sqrt{\left(\frac{\lambda_n^2}{\alpha_1}-\beta_m^2\right)}}{k_2\sqrt{\left(\frac{\lambda_n^2}{\alpha_2}-\beta_m^2\right)}}\sin\sqrt{\left(\frac{\lambda_n^2}{\alpha_1}-\beta_m^2\right)}h\sin\sqrt{\left(\frac{\lambda_n^2}{\alpha_2}-\beta_m^2\right)}(h-z)\right]^2\mathrm{d}z. \tag{A.6}$$

The characteristic values β_m and λ_n are positive roots of the following equations, respectively:

$$J_1(\beta_m r_0)=0, \tag{A.7}$$

$$k_1\sqrt{\left(\frac{\lambda_n^2}{\alpha_1}-\beta_m^2\right)}\tan\sqrt{\left(\frac{\lambda_n^2}{\alpha_1}-\beta_m^2\right)}h+k_2\sqrt{\left(\frac{\lambda_n^2}{\alpha_2}-\beta_m^2\right)}\tan\sqrt{\left(\frac{\lambda_n^2}{\alpha_2}-\beta_m^2\right)}(H-h)=0. \tag{A.8}$$

For the dimensionless temperature fields, the coefficient $A_0^*(\beta_m^*,\lambda_n^*,t^*)$ and norm are given as

$$A_0^*\left(\beta_m^*,\lambda_n^*,t^*\right)=\frac{\int_0^{r_0^*}J_0\left(\beta_m^*r^*\right)\left[f+(1-f)r^{*2}\right]\mathrm{e}^{-r^{*2}}r^*\,\mathrm{d}r^*\int_{\tau^*=0}^{t^*}\mathrm{e}^{-\lambda_n^{*2}(t^*-\tau^*)}Y(\tau^*)\,\mathrm{d}\tau^*}{J_0^2\left(\beta_m^*r_0^*\right)N\left(\beta_m^*,\lambda_n^*\right)}, \tag{A.9}$$

$$N\left(\beta_m^*,\lambda_n^*\right)=\int_0^{z_h^*}\cos^2\left[\cos\sqrt{\left(\lambda_n^{*2}-\beta_m^{*2}\right)}z^*\right]\mathrm{d}z^*+\gamma\int_{z_h^*}^{z_H^*}\left[\cos\sqrt{\left(\alpha\lambda_n^{*2}-\beta_m^{*2}\right)}\left(z_h^*-z^*\right)\times\cos\sqrt{\left(\lambda_n^{*2}-\beta_m^{*2}\right)}z_h^*+K\frac{\sqrt{\left(\lambda_n^{*2}-\beta_m^{*2}\right)}}{\sqrt{\left(\alpha\lambda_n^{*2}-\beta_m^{*2}\right)}}\sin\sqrt{\left(\lambda_n^{*2}-\beta_m^{*2}\right)}z_h^*\sin\sqrt{\left(\alpha\lambda_n^{*2}-\beta_m^{*2}\right)}\left(z_h^*-z^*\right)\right]^2\mathrm{d}z^*. \tag{A.10}$$

Appendix B

In this appendix, the equilibrium equations in the form of elastic displacement and electric potential are given as

$$c_{11}\left(\frac{\partial^2}{\partial r^2}+\frac{1}{r}\frac{\partial}{\partial r}\right)u-c_{11}\frac{u}{r^2}+c_{44}\frac{\partial^2 u}{\partial z^2}+(c_{13}+c_{44})\frac{\partial^2 w}{\partial r\partial z}+(e_{15}+e_{31})\frac{\partial^2\varphi}{\partial r\partial z}-\lambda_{11}\frac{\partial\Theta}{\partial r}=0, \tag{B.1}$$

$$(c_{13}+c_{44})\frac{\partial}{\partial z}\left(\frac{\partial u}{\partial r}+\frac{u}{r}\right)+c_{44}\frac{\partial^2 w}{\partial r^2}+c_{33}\frac{\partial^2 w}{\partial z^2}+c_{44}\frac{1}{r}\frac{\partial w}{\partial r}+e_{15}\left(\frac{\partial^2\varphi}{\partial r^2}+\frac{1}{r}\frac{\partial\varphi}{\partial r}\right)+e_{33}\frac{\partial^2\varphi}{\partial z^2}-\lambda_{33}\frac{\partial\Theta}{\partial z}=0, \tag{B.2}$$

$$(e_{15}+e_{31})\frac{\partial}{\partial z}\left(\frac{\partial u}{\partial r}+\frac{u}{r}\right)+e_{15}\left(\frac{\partial^2 w}{\partial r^2}+\frac{1}{r}\frac{\partial w}{\partial r}\right)+e_{33}\frac{\partial^2 w}{\partial z^2}-\epsilon_{11}\left(\frac{\partial^2\varphi}{\partial r^2}+\frac{1}{r}\frac{\partial\varphi}{\partial r}\right)-\epsilon_{33}\frac{\partial^2\varphi}{\partial z^2}+p_3\times\frac{\partial\Theta}{\partial z}+p_1\left(\frac{\partial\Theta}{\partial r}+\frac{\Theta}{r}\right)=0, \tag{B.3}$$

where the variables u, w and φ are the basic unknown functions.

Substituting Eq. (11) into Eqs. (B.1)–(B.3), we have the following relationships:

$$\begin{aligned}
&\frac{\partial}{\partial r}\sum_{j=1}^{4}\left(c_{11}\psi_{j,rr}+c_{11}\frac{1}{r}\psi_{j,r}+M_j\psi_{j,zz}\right)=\lambda_{11}\frac{\partial\Theta_1}{\partial r},\\
&\frac{\partial}{\partial z}\sum_{j=1}^{4}\left(N_j\psi_{j,rr}+N_j\frac{1}{r}\psi_{j,r}+P_j\psi_{j,zz}\right)=\lambda_{33}\frac{\partial\Theta_1}{\partial z},\\
&\frac{\partial}{\partial z}\sum_{j=1}^{4}\left(F_j\psi_{j,rr}+F_j\frac{1}{r}\psi_{j,r}+G_j\psi_{j,zz}\right)=-p_3\frac{\partial\Theta_1}{\partial z}-p_1\left(\frac{\partial\Theta_1}{\partial r}+\frac{\Theta_1}{r}\right).
\end{aligned} \tag{B.4}$$

Here, ψ is taken as $\psi_4=\psi$. The potential function ψ is chosen as the particular solution of the non-homogeneous equation with $p_1=0$, one should have the following relationships:

$$\frac{M_j}{c_{11}}=\frac{P_j}{N_j}=\frac{G_j}{F_j}=\gamma_j^2=\xi_j,\quad j=1,2,3, \tag{B.5}$$

$$\frac{\lambda_{11}}{c_{11}-M_4}=\frac{p_3}{G_4-F_4}=\frac{\lambda_{33}}{N_4-P_4}=\left(\frac{\lambda_n^2}{\alpha_1}-\beta_m^2\right)D_m(\beta_m,\lambda_n). \tag{B.6}$$

From Eq. (B.5), we can obtain a cubic algebra equation of ξ_j (Zhao et al., 1997; Wang and Zheng, 1995),

$$A\xi^3+B\xi^2+C\xi+D=0, \tag{B.7}$$

where, the coefficients are written as,

$$\left.\begin{aligned}
A&=e_{15}^2+c_{44}\epsilon_{11}\\
B&=\left(2e_{15}^2c_{13}-c_{44}e_{31}^2+2e_{15}e_{31}c_{13}-2e_{15}c_{11}e_{33}+\epsilon_{11}c_{13}^2+2c_{13}c_{44}\epsilon_{11}-c_{33}c_{11}\epsilon_{11}-c_{44}c_{11}\epsilon_{33}\right)/c_{11}\\
C&=\left[e_{33}(c_{11}e_{33}+2e_{15}c_{44})-2e_{33}(e_{15}+e_{31})(c_{13}+c_{44})-\epsilon_{33}\left(c_{13}^2+2c_{13}c_{44}-c_{33}c_{11}\right)+\epsilon_{11}c_{33}c_{44}+c_{33}(e_{15}+e_{31})^2\right]/c_{11}\\
D&=-\left(e_{33}^2+\epsilon_{33}c_{33}\right)c_{44}/c_{11}
\end{aligned}\right\}. \tag{B.8}$$

The constants l_{ij} $(i = 1, 2, j = 1, 2, 3)$ and the relationships among l_{14}, l_{24} and $D_m(\beta_m, \lambda_n)$ can be completely determined from Eq. (B.6). The related constants $(F_j, G_j, M_j, N_j, P_j,\ j = 1, 2, 3, 4)$ are given as,

$$\left.\begin{aligned} M_j &= c_{44} + (c_{13} + c_{44})l_{1j} + (e_{31} + e_{15})l_{2j} \\ N_j &= c_{13} + c_{44}(1 + l_{1j}) + e_{15}l_{2j} \\ P_j &= c_{33}l_{1j} + e_{33}l_{2j} \\ F_j &= e_{15}(1 + l_{1j}) + e_{31} - \epsilon_{11}l_{2j} \\ G_j &= e_{33}l_{1j} - \epsilon_{33}l_{2j} \end{aligned}\right\}. \tag{B.9}$$

The corresponding factors of thermopiezoelectric fields are written as,

$$\left.\begin{aligned} a_i &= c_{44}(1 + l_{1i}) + e_{15}l_{2i} \\ b_i &= c_{33}l_{1i} + e_{33}l_{2i} - c_{13}\gamma_i^2 \\ c_i &= e_{33}l_{1i} - \epsilon_{33}l_{2i} - e_{31}\gamma_i^2 \\ d_i &= c_{13}l_{1i} + e_{31}l_{2i} - c_{11}\gamma_i^2 \\ f_i &= c_{13}l_{1i} + e_{31}l_{2i} - c_{12}\gamma_i^2 \\ g_i &= e_{15}(1 + l_{1i}) - \epsilon_{11}l_{2i} \end{aligned}\right\}. \tag{B.10}$$

References

Ashida, F., Tauchert, T.R., Noda, N., 1994. Potential function method for piezothermoelastic problems of solids of crystal class 6 mm in cylindrical coordinates. J. Therm. Stresses 17, 361–375.

Cheng, S.D., Kam, C.H., Zhou, Y., Que, W.X., Lam, Y.L., Chan, Y.C., Gan, W.S., 2000. Sol–gel derived nanocrystalline thin films of $PbTiO_3$ on glass substrate. Thin Solid Films 375, 109–113.

Choi, W.K., Choi, S.K., Lee, H.M., 1999. Relationship between domain structure and film thickness in epitaxial $PbTiO_3$ films deposited on MgO(0 0 1) by reactive sputtering. J. Mater. Res. 14 (12), 4677–4684.

Crawley, E.F., de Luis, J., 1987. Use of piezoelectric actuators as elements of intelligent structures. AIAA J. 25 (10), 1373–1385.

Duan, Z.P., Zhou, Y.C., Huang, C.G., 1995. On laser-induced reverse plugging effect. Acta Mech. Sinica 11 (3), 239–250.

Duan, Z.P., Zhou, Y.C., Xie, B.M., 1996. The analytical study on the laser induced reverse plugging effect by using the classical elastic plate theory (II)-reverse bulging. Appl. Math. Mech. 17 (7), 607–620.

Evans, A.G., Hutchinson, J.W., 1995. The thermomechanical integrity of thin films and multilayers. Acta Metall. Mater. 43 (7), 2507–2530.

Haertling, G.H., 1999. Ferroelectric ceramics: history and technology. J. Am. Ceram. Soc. 82 (4), 797–818.

Hector, L.G.J., Hetnarski, R.B., 1996. Thermal stresses due to a laser pulse: elastic solution. Trans. ASME J. Appl. Mech. 63, 38–46.

Hutchinson, J.W., Suo, Z., 1992. Mixed mode cracking in layered materials. Adv. Appl. Mech. 29, 63–191.

Iesan, D., 1989. On some Theorems in Thermopiezoelectricity. J. Therm. Stresses 12, 209–223.

Im, S., Atluri, S.N., 1989. Effects of a piezo-actuator on a finitely deformed beam subjected to general loading. AIAA J. 27 (12), 1801–1807.

Kant, R., 1988. Laser induces heating of a multilayered medium resting on a half-space: Part 1—stationary source. Trans. ASME J. Appl. Mech. 55, 93–97.

Mindlin, R.D., 1974. Equations of high frequency vibrations of thermopiezoelectric crystal plates. Int. J. Solids Structures 10, 625–637.

Nonhof, C.J., 1988. Materials Processing with Nd-Lasers. Electrochemical Publications Ltd, Ayr. Scotland.

Nowacki, W., 1978. Some general theorems of thermopiezoelectricity. J. Therm. Stresses 1, 171–182.

Özisik, M.N., 1993. Heat Conduction, second ed. Wiley, New York.

Sakashita, Y., Ono, T., Segawa, H., Tominaga, K., Okada, M., 1991. Preparation and electrical properties of MOCVD-deposited PZT thin films. J. Appl. Phys. 69 (12), 8352–8357.

Setter, N., Colla, E.L., 1993. Ferroelectric Ceramics. Birkhäuser Verlag, Basel, Boston, Berlin.

Shang, F.L., Wang, Z.K., Li, Z.H., 1996. Thermal stresses analysis of a three-dimensional crack in a thermopiezoelectric solid. Engng. Fract. Mech. 55 (5), 737–750.

Steen, W.M., 1991. Laser Material Processing. Springer-Verlag, New York.

Verardi, P., Dinescu, M., Craciun, F., Sandu, V., 1997. Oriented $PbZr_xTi_{1-x}O_3$ thin films obtained at low substrate temperature by pulsed laser deposition. Thin Solid Films 311, 171–176.

Volchenok, I.A, Rudin, G.I., 1988. Thermoelastic stresses in a multilayer plate upon action of laser radiation. J. Engng. Phys. 55 (5), 1286–1290.

Wang, X.D., Meguid, S.A., 2000. On the electroelastic behaviour of a thin piezoelectric actuator attached to an infinite host structure. Int. J. Solids Structures 37, 3231–3251.

Wang, Z.K., Zheng, B.L., 1995. The general solution of three-dimensional problems in piezoelectric media. Int. J. Solids Structures 32 (1), 105–115.

Welsh, L.P., Tuchman, J.A., Herman, I.P., 1988. The importance of thermal stresses and strains induced in laser processing with focused Gaussian beam. J. Appl. Phys. 64 (11), 6274–6286.

Xu, Y.H., 1991. Ferroelectric Materials and Their Applications. Elsevier Science Publishing Company, New York.

Zhao, M.H., Shen, Y.P., Liu, Y.J., Liu, G.N., 1997. Isolated crack in three-dimensional piezoelectric solid: Part I—solution by Hankel transform. J. Theor. Appl. Fract. Mech. 26, 129–139.

Zhou, Y.C., Duan, Z.P., 1996. Circular brass foil failed by plugging opposite to direction of incident laser beam. Theoretical Appl. Fract. Mech. 24 (2), 135–138.

Zhou, Y.C., Duan, Z.P., Xie, B.M., 1997. Long pulsed laser induced reverse bulging and plugging. Int. J. Engng. Sci. 35, 613–621.

Zhou, Y.C., Duan, Z.P., Yang, Q.B., 1998. Shear deformation analysis on laser-induced reverse bulging and plugging. Int. J. Non-Linear Mech. 33 (3), 433–446.

Zhou, Y.C., Hashida, T., in press. Delamination cracking in thermal barrier coating system. Trans. ASME J. Engng. Gas Turbines Power.

Zhu, W., Liu, Z.Q., Lu, W., Tse, M.S., Tan, H.S., Yao, X., 1996. A systematic study on structural and dielectric properties of lead zirconate titanate/(Pb, La)($Zr_{(1-x)}Ti_{(x)}O_3$ thin films deposited by metalloorganic decomposition technology. J. Appl. Phys. 79 (8), 4283–4290.